OPEN ACCESS Science International

ISSN 2305-1884
DOI: 10.17311/sciintl.2017.155.163

Research Article
Effect of Gamma Radiation on the Crystallographic Features and Applications of Stannic Antimonate and Its Dopants

Mamdouh Mohamed Abou-Mesalam and Asmaa Bendary Ibrahim

Atomic Energy Authority, Hot Labs. Centre, P. Code 13759, Cairo, Egypt

Abstract

Objective: Doping of inorganic ion-exchange material stannic antimonates with cobalt and strontium ions by sol-gel technique was conducted for a novel ion-exchangers. **Methodology:** Undoped and doped stannic antimonates has been characterized by elemental analysis (X-ray fluorescence), fourier transform infrared spectroscopy (FT-IR), thermal analysis and X-ray diffraction studies. X-ray peak broadening analysis was used to evaluate the crystallite size and lattice strain by Scherrer's formula and Williamson-Hall (W.H) analysis. **Results:** The structures of three ion-exchangers were identified and the empirical formulas found as ($SnSb.O_{(1.59)}.3.34H_2O$), ($CoSnSb.O_{(1.51)}.4.18H_2O$) and ($SrSnSb.O_{(1.5)}.H_2O$) for stannic antimonate, cobalt stannic antimonate and strontium stannic antimonate, respectively. Undoped and doped stannic antimonates as inorganic ion-exchangers were subjected to gamma doses of 10, 50 and 100 kGy to study the radiation stabilities of these compounds. The total capacity for Co^{2+} and Cd^{2+} ions were studied for stannic antimonates, cobalt and strontium doped stannic antimonates. **Conclusion:** There were no practically significant changes between the control and irradiated samples, showing that these exchangers are stable up to the levels of irradiation under investigation.

Key words: Doping, inorganic ion-exchangers, crystallite size, lattice strain, stannic antimonate

Citation: Mamdouh Mohamed Abou-Mesalam and Asmaa Bendary Ibrahim , 2017. Effect Of gamma radiation on the crystallographic features and applications of stannic antimonate and its dopants. Sci. Int., 5: 155-163.

Corresponding Author: Mamdouh Mohamed Abou-Mesalam, Atomic Energy Authority, Hot Labs. Centre, P. Code 13759, Cairo, Egypt Tel: 00201224506010

Competing Interest: The authors have declared that no competing interest exists.

Data Availability: All relevant data are within the paper and its supporting information files.

INTRODUCTION

Antimonate salts are one of the most important classes of synthetic inorganic ion exchange materials as they are temperature resistant and stable under chemical attacks[1-3]. Some inorganic and organic materials show bad effect on the crystallographic features when exposed to high radiation doses. The main problem was shown in laboratory, prepared some salts of poly basic acids with tetravalent metal ions such as cerium (IV)-, tin (IV)-, titanium (IV)- and silicon (IV) antimonates[3-7] under different conditions and study their possible use in the treatment of low and intermediate-level radioactive liquid wastes[3-7]. X- ray profile analysis is a simple and tool to estimate the crystallite size and lattice strain[8]. Among the available methods to estimate the crystallite size and lattice strain are the pseudo-Voigt function, riveted refinement and Warren-Averbach analysis[9-11]. Williamson Hall (W.H) analysis is a simplified integral breadth method where both size-induced and strain–induced broadening is deconvoluted by considering the peak width as a function of 2θ peak width Arora and Vashali[12]. The two main properties extracted from peak width analysis are (a) crystallite size and (b) lattice strain. Crystallite size is a measure of the size of a coherently diffracting domain. The crystallite size of the particles is not generally the same as the particle size due to the presence of polycrystalline aggregates[13]. Lattice strain is a measure of the distribution of lattice constants arising from crystal imperfections, such as lattice dislocation. The other sources of strain are the grain boundary triple junction, contact or sinter stresses, stacking faults, coherency stresses, etc.[14-15]. The aim of this study was to prepare and characterize stannic antimonate, cobalt and strontium doped stannic antimonates as inorganic ion exchangers. The crystallite size and lattice strain due to dopping of cobalt and strontium with stannic antimonate was investigated. The empirical formulas, structures and the ion-exchange capacities of the product materials were conducted.

MATERIALS AND METHODS

Synthesis of stannic antimonate (SnSb) ion exchanger: Stannic antimonate was synthesized by the reaction of 0.1M stannic tetra chloride (dissolved in distilled water) with 0.1 M antimony metal (dissolved in aqua regia) with molar ratio Sn to Sb equal 1:1. During the addition process, yellow gelatinous precipitate formed. After complete addition, few drops of diluted ammonia solution were added for complete precipitation, the precipitate left overnight standing and the mixture was hydrolyzed in distilled water and left for 2 days at room temperature. The precipitate formed was separated by centrifugation at 3000 rpm for 5 min. The precipitate was washed by 0.5M HNO_3 to be free from Cl^- ions and rewashed by distilled water to remove NO_3^-. The precipitate was dried at 60°C in a drying oven and washed with hot water (70°C) to remove the air traps in the solid and then redried at 60°C. The solid was ground, sieved to mesh size and stored at room temperature.

Synthesis of cobalt and/or strontium stannic antimonates (CoSnSb or SrSnSb) ion exchangers: Cobalt and/or strontium chloride solutions with concentration 0.1 M were used for doped cobalt and/or strontium *in-situ* stannic-antimonates. Cobalt and/or strontium stannic-antimonate solid samples were prepared by the reaction of 0.1 M cobalt and/or strontium chloride solutions with a mixture of 0.1 M stannic tetra chloride (dissolved in distilled water) and 0.1 M antimony metal (dissolved in aqua regia) with volumetric molar ratio Co and/or Sr :Sn to Sb equal 1:1:1. The reaction carried out in water bath at 60°C with continuous stirring for 4 h. Gelatinous precipitates formed during the addition process of cobalt and/or strontium chloride solutions to the mixture. After an overnight standing the precipitates separated by centrifugation at 3000 rpm. The solids treated by 0.1 M HNO_3^- to remove impurities and Cl^- ions. Solids rewashed with distilled water to remove NO_3^- ions. After drying in drying oven at 60°C, the granules solids poured in near boiling water at 70-80°C to remove the trapped air. Dry, grand, sieve and store solids at room temperature.

Characterization of synthesized stannic antimonate and doping stannic antimonates: Fourier transform infrared spectra (FT-IR) for synthesized materials were measured using Bomem FTIR spectrometer model BOMEM, MBSeries. The measurement carried out by KBr disc method technique from 400-4000 cm^{-1}. X-ray diffraction patterns (XRD) of the synthesized materials were recorded using Shimadzu XD-D1 spectrometer with CuK_α radiation tube ($\lambda = 1.5418$ Å) and 30 Kv, 30 mA. The patterns and the intensity width-spacing value tables printed out for calculation of the crystallite size and strain of the samples. The crystal system for the structure was determined. Thermal analysis was measured using a Shimadzu DT-60 thermal analyzer, Japan, at a heating rate of 15 min. under a nitrogen atmosphere. An elemental analysis for the synthesized materials investigated by X-ray fluorescence technique, Philips-ray fluorescence PW-2400

sequential spectrometer. Samples were prepared for measurement process as reported earlier by El-Naggar *et al.*[13] grained 1.0 g of the solid sample to very fine particles and mixed with poly vinyl metha-acrylate as a binder to facilitate the pressing process. The mixture pressed in pressing machine to 20 psi for 30 sec. The measurement carried out using super quantitative analysis program.

Capacity measurements: The capacity of synthesized stannic antimonate and doping stannic antimonate for Co^{2+} and Cd^{2+} ions were determined by the repeated batch technique, by equilibrating nearly 0.7 g of stannic antimonate and doping stannic antimonate with 70 mL of (30 ppm) Co^{2+} and Cd^{2+} ions solutions on a shaker thermostat adjusted at 25±1°C. After an equilibrium, the solution was separated and repeated until no further sorption occurs. The capacity was calculated using the following Eq:

$$\text{Capacity in (mg g}^{-1}) = \frac{\text{Uptake}}{100} \times \frac{V}{m} \times Co \times 100 \quad (1)$$

$$\text{Uptake (\%)} = \frac{A_o - A}{A_o} \times 100 \quad (2)$$

Where:

A_o and A = Initial and final concentrations of solution
C_o = Initial concentration of solution
V = Solution volume (mL)
m = Weight of the exchanger (g)

Irradiation of the ion exchanger: The samples were irradiated with gamma rays by using Egypt Mega I irradiation facility (type J -6300 Atomic Energy Canada). It was conducted for variable time periods in order to cover a range of absorbed doses 10, 50 and 100 kGy. The experiments described later were performed before and immediately after irradiation of the samples.

RESULTS AND DISCUSSION

Fourier transforms infrared spectroscopy: The effect of γ-radiation on the structure of synthesized stannic antimonate and doping stannic antimonate are shown in Fig. 1a-c. Figure 1(a-c) showed the IR spectra of unirrdiated and irradiated stannic antimonite and doping stannic antimonate. The data in Fig. (1a-c) showed partially there is very little difference between original and irradiated stannic antimonate and doping stannic antimonate. In case of stannic antimonite (Fig. 1a) the investigated bands at ~(3600-2800) may be due to the free water molecules present in the texture of stannic-antimonate[16-18] are decreased by exbosing the sample of stannic antimonate and doping stannic antimonite to γ-radiation with dose 10, 50 and 100 kGy. The peaks at ~2455 and ~1652 cm^{-1} may be due to CO_2 in the atmosphere and interstitial water(bonded water), respectively[16-18]. The peaks at ~1110, 754 cm^{-1} shown in (Fig. 1a-c) may be due to Sn-O bonds[19]. The peaks at 500 and 400 cm^{-1} are due to Sb-O bond[19] and characterized to antimonate groups. These peaks not affected by γ-radiation. Figure (1a-c) show the IR spectra of original and irradiated stannic antimonate and doping stannic antimonite samples. These figures indicated that there is no notified difference between the original and irradiated stannic antimonate and doping stannic antimonite samples.

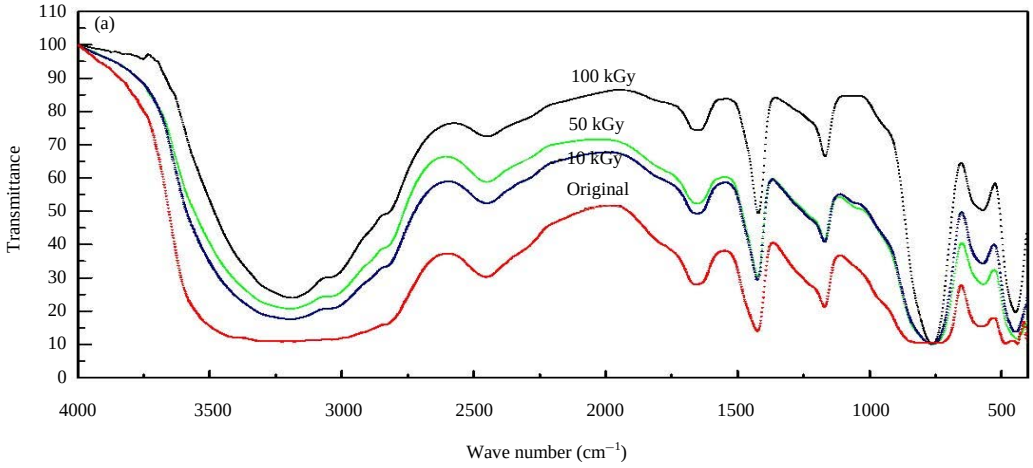

Fig. 1(a-c): Continue

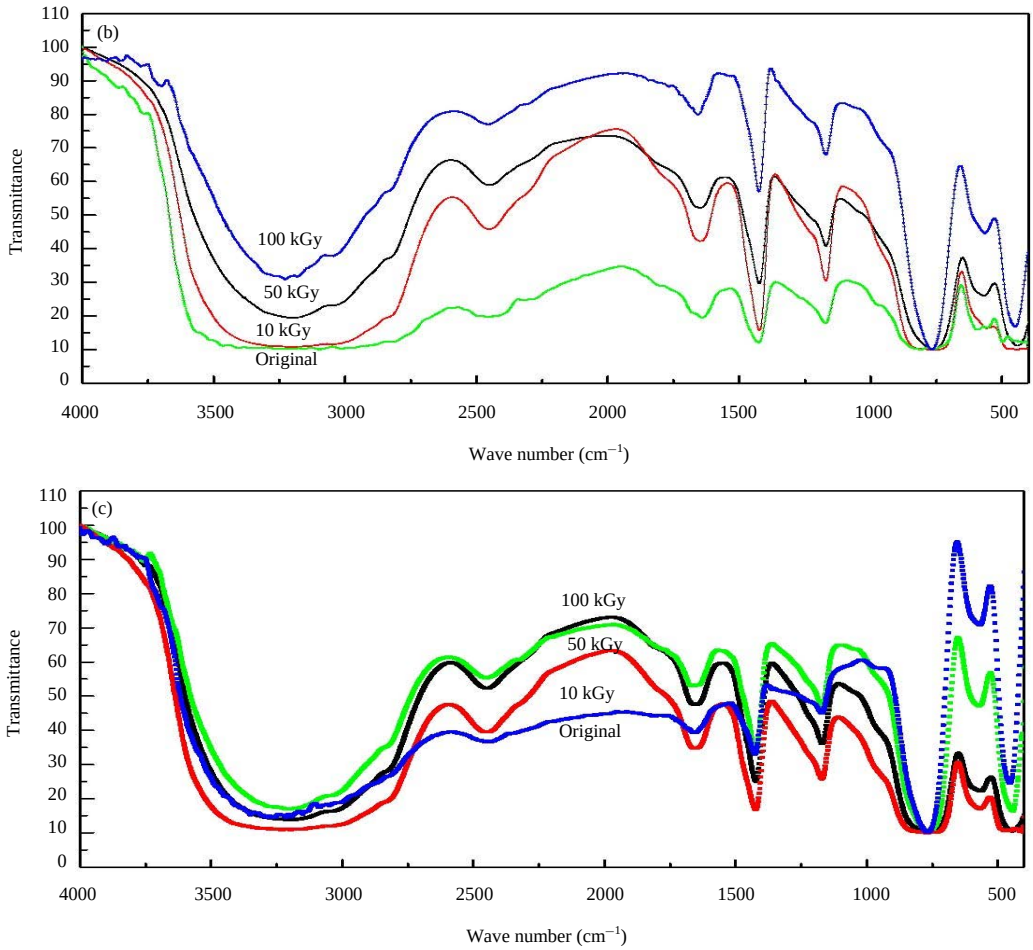

Fig. 1(a-c): (a) IR spectra of original and irradiated stannic antimonate (SnSb), (b) IR spectra of original and irradiated cobalt stannic antimonate (CoSnSb) and (c) IR spectra of original and irradiated strontium stannic antimonate (SrSnSb)

Table 1: Total weight loss occurred from room temperature to 1000°C amounts for stannic antimonate and doping stannic antimonate

Ion exchanger	SnSb		CoSnSb		SrSnSb	
γ-dose (kGy)	0	100	0	100	0	100
Weight loss (%)	20.02	29.02	20.09	24.17	21.44	29.89

Thermal analysis: DTA and TGA thermograms of stannic antimonate and doping stannic antimonate are represented in Fig. (2a-c and 3a-c). DTA of stannic antimonate indicated a prominent endothermic peak at ~283.35°C that may be due to free adsorbed water. The broad exothermic peak at ~/337.07°C may be due to the decomposition of residual -OH groups and condensation of non-bonded oxygen. The broad endothermic peak at ~431.69°C corresponds to crystallization of metal oxides[16]. From TG curve it is evident that stannic antimonate was thermally stable up to the temperature of 1000°C. The total weight loss occurred from room temperature to 1000°C amounts are indicated in Table 1.

The loss of ignition that means the water content was calculated from the calcination of an ion exchange material at 1000°C. The data in Table 1 indicated that the weight loss due to ignition were equal 20.02, 20.09 and 21.44 for SnSb, CoSnSb and SrSnSb, respectively. This value was used in calculation of the number of water molecules in the material using the Eq. 1[17]:

$$18n = \frac{X\,(M+18n)}{100} \quad (3)$$

Where:
X = Percent weight loss of ignition
M = Molecular weight of the material

The elemental analysis of the material for Co, Sr, Sn and Sb elements was carried out by X-ray fluorescence technique. From all results obtained from IR, DTA, XRD and XRF, the

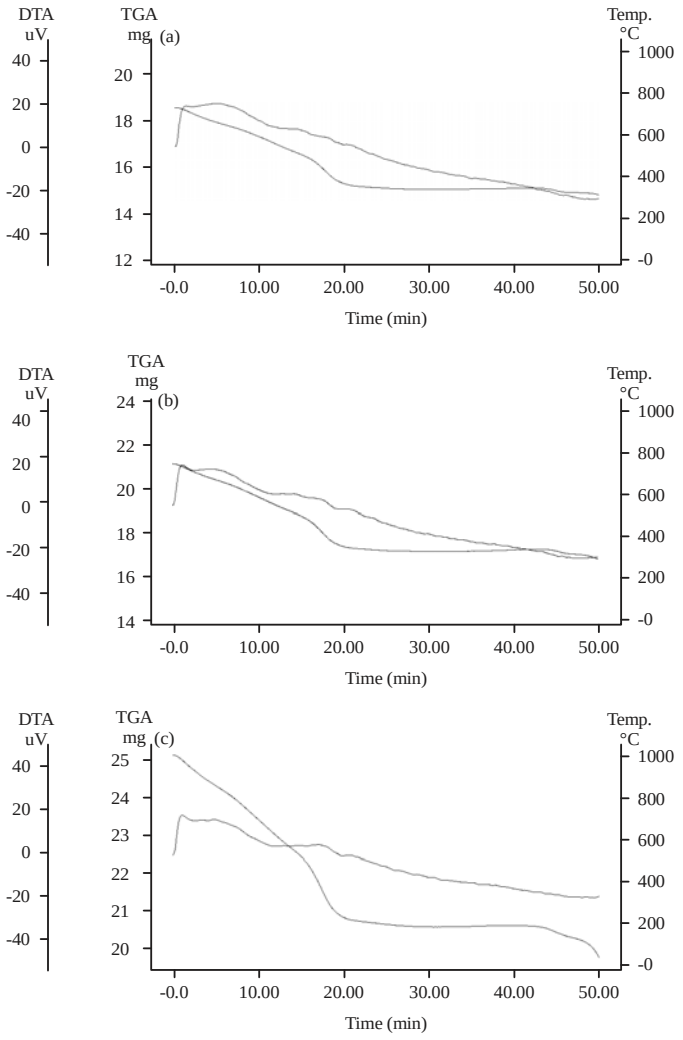

Fig. 2(a-c): (a) Differential thermal and thermogravimetric spectra of original stannic antimonate, (b) Differential thermal and thermogravimetric spectra of original cobalt stannic antimonate and (c) Differential thermal and thermogravimetric spectra of original strontium stannic antimonate

tentative formula of stannic antimonate, cobalt stannic antimonate and strontium stannic antimonate material was assigned to ($SnSb.O_{(1.59)}.nH_2O$) ,($CoSnSb.O_{(1.51)}.nH_2O$) and ($SrSnSb.O_{(1.5)}.nH_2O$), respectively. From the loss of ignition, the number of water molecules (n) per mole of the material was calculated and the above formulas then rewritten as ($SnSb.O_{(1.59)}.3.34H_2O$),($CoSnSb.O_{(1.51)}.4.18H_2O$) and ($SrSnSb.O_{(1.5)}.4.97H_2O$), respectively, for the structure modeling and the arrangement.

X-effect of gamma radiation on crystallographic feature of SnSb and M-SnSb: Figure 4a-c show the XRD patterns of stannic antimonate and doping stannic antimonate. These figures show different peaks at different 2θ with variable intensities indicating the crystalline nature of these materials. The brage angle 2θ and the full width at half maximum β(FWHM) were determined to evaluate the crystallite size and lattice strain of these materials.

From Debye-Scherrer's formula:

$$D = \frac{K.\lambda}{\beta.\text{Cos}\ \theta} \quad (4)$$

Where:
D = Effective average crystalline size
K = Shape factor (0.89)
λ = Wavelength of CuKα radiation in nanometer

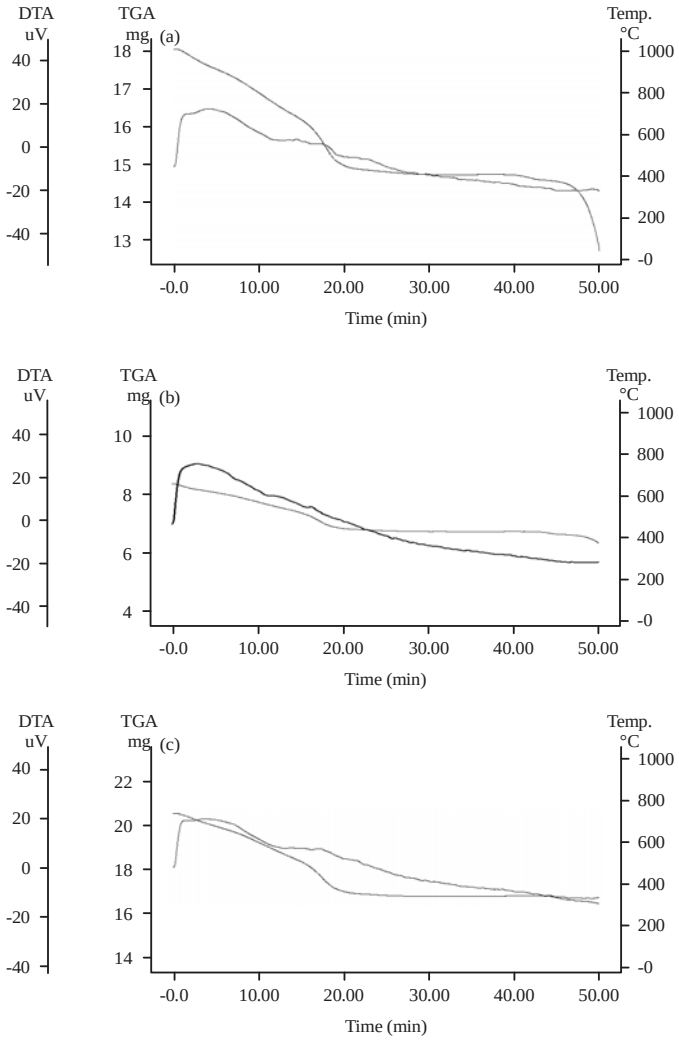

Fig. 3(a-c): (a) Differential thermal and thermogravimetric spectra of irradiated stannic antimonate at 100 kGy, (b) Differential thermal and thermogravimetric spectra of irradiated cobalt stannic antimonate at 100 kGy and (c) Differential thermal and thermogravimetric spectra of irradiated strontium stannic antimonate at 100 kGy

θ = Bragg diffraction angle
β = Measured full width at half maximum (FWHM)

The lattice strain induced in powders due to crystal imperfection and distortion was calculated using Hall equation with the formula[20,21]:

$$\frac{\beta.\text{Cos}\,\theta}{\lambda} = \frac{1}{D} + \frac{\varepsilon.\text{Sin}\,\theta}{\lambda} \quad (5)$$

Where:
ε = Effective strain

By substitution in Eq. 3 from equation 1 about the value of (ε) Eq. 5 becomes:

$$\frac{\beta.\text{Cos}\,\theta}{\lambda} = \left\{\frac{\beta.\text{Cos}\,\theta}{K.\lambda} + \frac{\varepsilon.\text{Sin}\,\theta}{\lambda}\right\} \quad (6)$$

By multiplying both sides of Eq. 6 in constant value {λ/(β.Cos θ)} and rearrangement we get on:

$$\varepsilon = \frac{\beta}{4\text{Tan}\,\theta} \quad (7)$$

From Eq. 3 and 6, it was confirmed that the peak width from crystallite size varies as 1/Cos θ strain varies as tan θ.

Assuming that the particle size and strain contributions to line broadening are independent to

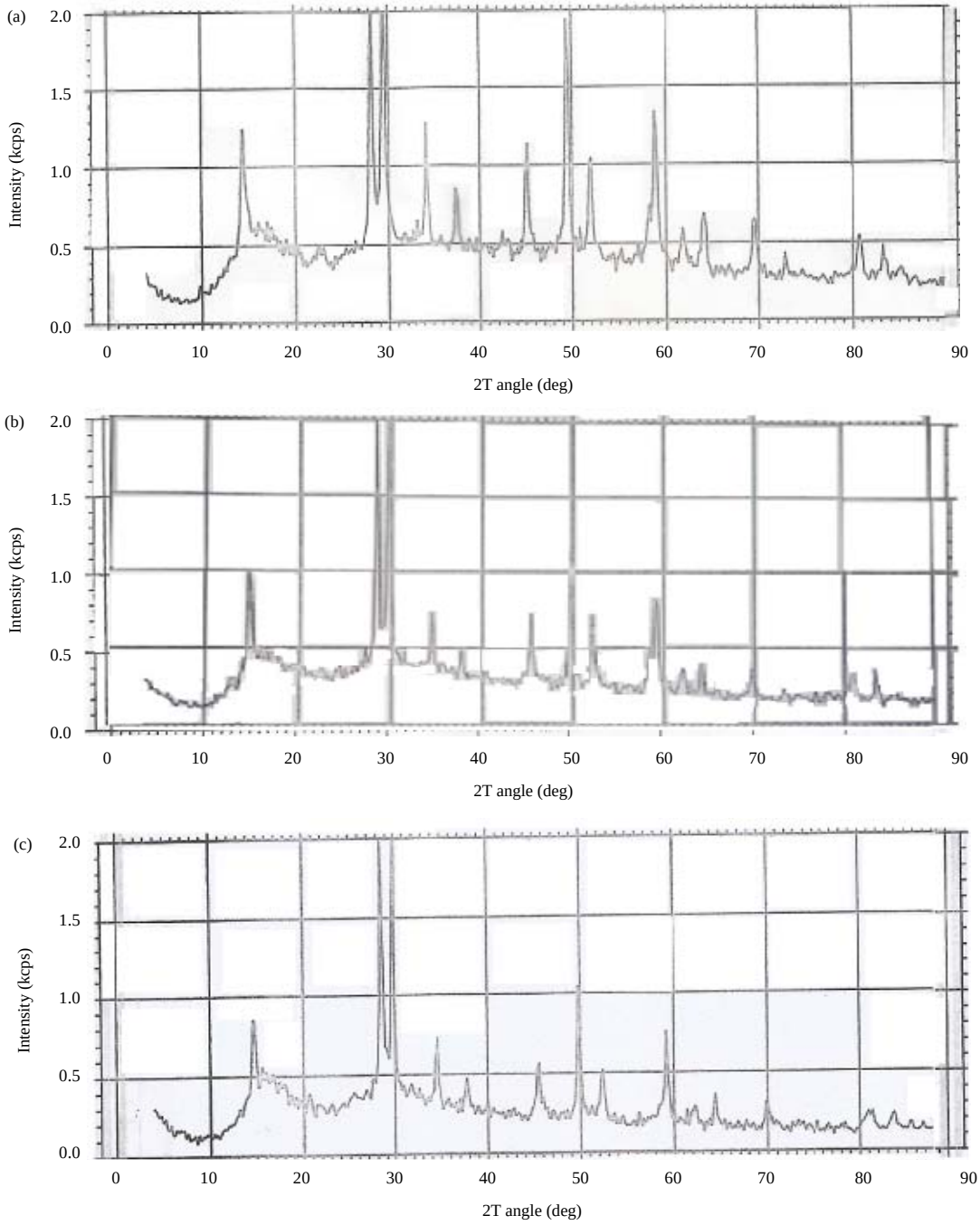

Fig.4(a-c): (a) X-ray diffraction patterns of stannic antimonate at 0 radiation, (b) X-ray diffraction patterns of cobalt stannic antimonate at 0 radiation and (c) X-ray diffraction patterns of Strontium stannic antimonate at 0 radiation

each other and both have a Cauchy-like profile, the observed line breadth is simply the sum of Eq. 4 and 7:

$$B = \frac{K.\lambda}{D \cos \theta} + 4 \varepsilon \tan \theta \quad (8)$$

By rearranging the above equation, we get:

$$\beta .\cos = \frac{K.\lambda}{D} + 4 \varepsilon \sin \theta \quad (9)$$

The above equations are Williamson-Hall's (W-H) equations.

Table 2: Crystallite size and lattice strain for stannic antimonate and doping stannic antimonate

Ion exchanger	kGy	D (Crystallite size, nm)×10^{-2}	Lattice strain (ε)
SnSb	0	10.38	0.3571
	10	14.43	0.3333
	50	14.90	0.2857
	100	15.15	0.2272
CoSnSb	0	16.13	0.263
	10	16.32	0.1923
	50	16.32	0.1818
	100	18.78	0.11
SrSnSb	0	16.32	0.1724
	10	17.81	0.1429
	50	18.53	0.1351
	100	20.46	0.1042

Table 3: Effect of gamma radiation on capacity of SnSb and M-SnSb at 25±1°C

Ion exchanger	Capacity (mg g^{-1})											
	SnSb				CoSnSb				SrSnSb			
γ-dose Kgy ion	0	10	50	100	0	10	50	100	0	10	50	100
Co^{2+}	9.54	9.85	10.12	10.36	10.74	11.04	11.14	11.52	11.7	11.6	12.0	12.3
Cd^{2+}	12.80	14.50	15.30	14.20	15.40	16.30	16.70	17.30	17.7	17.1	17.6	18.1

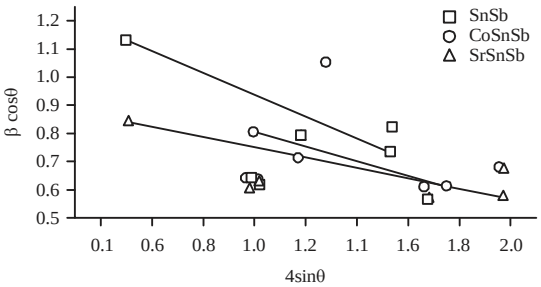

Fig. 5: Plots of β cos θ against 4 sinθ for SnSb and dopping SnSb ion exchangers

By plots the relation between (4 Sin θ) along the x-axis and (β.Cos θ) along the y-axis as shown in Fig. 5 and from the linear fit of the data, the crystallite size was estimated from the y-intercept and the lattice strain (ε), from the slope of the fit was calculated and results represented in Table 2. The data in Table 2 indicated that the crystallite size of SnSb, CoSnSb and SrSnSb are 10.38×10^{-2}, 16.13×10^{-2} and 16.32×10^{2} nm, respectively, with the order SrSnSb>CoSnSb>SnSb.

From data in Table 2 crystallite size of cobalt stannic antimonate and strontium stannic antimonate are higher those of stannic antimonate that may be related to doping insitu precipitation of cobalt and strontium with stannic antimonite. Also Table 2 indicated that the strain in ion exchangers decreases as the crystallite size increased which is an unusual phenomenon[22].

Effect of gamma radiation on capacity of SnSb and M-SnSb: The ion exchange capacities of original and irradiated samples of SnSb and M-SnSb for Cd^{2+} and Co^{2+} ions were studied and the results were tabulated in Table 3. Table 3 showed that the capacity values increased for Cd^{2+} and Co^{2+} ions with increasing the irradiation doses. This increasing may be attributed to the mobility of Cd^{2+} and Co^{2+} ions, which increased with increasing the irradiation dosses.

CONCLUSION

Stannic antimonate, cobalt or strontium stannic antimonates prepared by sol-gel technique with an empirical formulas ($SnSb.O_{(1.59)}.3.34H_2O$), ($CoSnSb.O_{(1.51)}.4.18H_2O$) or ($SrSnSb.O_{(1.5)}.H_2O$) were prepared and subjected to gamma doses of 10, 50 and 100 kGy to study the radiation stabilities of these compounds. Crystallite size and lattice strain were evaluated by Scherrer's formula and Williamson-Hall (W.H) using X-ray peak broadening analysis. The total capacity for Co^{2+} and Cd^{2+} ions were calculated for stannic antimonates, cobalt and strontium doped stannic antimonates and found that there were no practically significant changes between the control and irradiated samples, showing that these exchangers are stable up to the levels of irradiation under investigation.

SIGNIFICANCE STATEMENT

This study discovered new materials such as stannic antimonate and its dopants and its resistance to radiation doses upto 100 kGy. Also, the study show high capacity for Co^{2+} and Cd^{2+} ions.

REFERENCES

1. Khan, A.M., S.A. Ganai and S.A. Nabi, 2009. Synthesis of a crystalline organic-inorganic composite exchanger, acrylamide stannic silicomolybdate: binary and quantitative separation of metal ions. Colloids Surf. Physicochem. Eng. Aspect, 337: 141-145.
2. Abou-Mesalam, M.M., M.R. Abass, M.A. Abdel-Wahab, E.S. Zakaria, A.M. Hassan and H.F. Khalil, 2016. Complex doping of d-block elements cobalt, nickel and cadmium in magneso-silicate composite and its use in the treatment of aqueous waste. Desalination Water Treat., 57: 25757-25764.
3. Abdel-Galil, E.A., A.B. Ibrahim and M.M. Abou-Mesalam, 2016. Sorption behavior of some lanthanides on polyacrylamide stannic molybdophosphate as organic-inorganic composite. Int. J. Ind. Chem., 7: 231-240.
4. El-Naggar, I.M., E.S. Zakaria, M.M. Abou-Mesalam and H.F. Aly, 1999. Removal of some radioactive nuclides by *in-situ* precipitation with ion exchange materials. Czechoslovak J. Phys., 49: 951-958.
5. El-Dessouky, M.I., S.I. El-Dessouky and M.M. Abou-Mesalam, 2000. Retention of some hazardous radionuclides from nitric acid solution using tin(IV) antimonate as a cation exchanger. Radiochim. Acta, 88: 101-106.
6. El-Naggar, I.M., M.M. Abou-Mesalam, M.M. Abdel-Hamid, S.A. Shady and H.F. Aly, 2000. Synthesis and adsorption behaviour of some organic and inorganic sorbents for some hazardous toxic elements. Proceedings of the 7th Conference on Nuclear Science and Applications, February 6-10, 2000, Cairo, Egypt, pp: 461-472.
7. El-Naggar, I.M., M.M. Abou-Mesalam and S.A. Shady, 2000. Ion exchange kinetics of Co^{2+} and Zn^{2+} ions in the particles of some organic and inorganic sorbents. Proceedings of the 7th Conference on Nuclear Science and Applications, February 6-10, 2000, Cairo, Egypt, pp: 37-45.
8. Teicher, B.A., J.L. Jacobs, K.N. Cathcart, M.J. Abrams, J.F. Vollano and D.H. Picker, 1987. Some complexes of cobalt(III) and iron(III) are radiosensitizers of hypoxic EMT6 cells. Radiat. Res., 109: 36-46.
9. Sharma, K., S.C. Joshi and R.V. Singh, 2000. Fertility inhibitor heterobimetallic complexes of platinum(II) and palladium(II): Synthetic, spectroscopic and antimicrobial aspects. Metal-Based Drugs, 7: 105-113.
10. Rafique, S., M. Idrees, A. Nasim, H. Akbar and A. Athar, 2010. Transition metal complexes as potential therapeutic agents. Biotechnol. Mol. Biol. Rev., 5: 38-45.
11. Bharti, D., C. Arora and G. Kaur, 2012. Antifungal screening of some transition metal ferrocyanides against *Aspergillus niger* and *Candida albicans*. Asian J. Chem., 24: 1061-1063.
12. Arora, C. and Vashali, 2009. Synergistic effect of antimicrobial constituents of *Vitex negundo* with metal ferrocyanides. Progr. Agric., 9: 31-34.
13. El-Naggar, I.M., M.M. Abou-Mesalam, M.M. El-Shorbagy and S.A. Shady, 2006. Thermal and chemical stabilities of some synthesized inorganic ion exchange materials. Arab J. Nucl. Sci. Applic., 39: 25-34.
14. Ungar, T., 2007. Characterization of nanocrystalline materials by X-ray line profile analysis. J. Mater. Sci., 42: 1584-1593.
15. Abou-Mesalam, M. and I. El-Naggar, 2009. Chemical deposition of zirconium doped tin silicate ion-exchanger and its characterization. J. Radioanal. Nucl. Chem., 279: 333-340.
16. Abou-Mesalam, M., 2002. Retention behavior of nickel, copper, cadmium and zinc ions from aqueous solutions on silico-titanate and silico-antimonate used as inorganic ion exchange materials. J. Radioanal. Nucl. Chem., 252: 579-583.
17. El-Nagarr, I.M. and M.M. Abou-Mesalam, 2007. Novel inorganic ion exchange materials based on silicates; synthesis, structure and analytical applications of magneso-silicate and magnesium alumino- silicate sorbents. J. Hazard. Mater., 149: 686-692.
18. Abou-Mesalam, M.M., 2003. Sorption kinetics of copper, zinc, cadmium and nickel ions on synthesized silico-antimonate ion exchanger. Colloids Surf. A: Physicochem. Eng. Aspects, 225: 85-94.
19. Nyquist, R.A. and R.O. Kagel, 1997. Infrared and Raman Spectra of Inorganic Compound and Organic Salts. Academic Press, New York.
20. Gu, F., S.F. Wang, M.K. Lu, G.J. Zhou, D. Xu and D.R. Yuan, 2004. Structure evaluation and highly enhanced luminescence of Dy^{3+}-doped ZnO nanocrystals by Li^{+} doping via combustion method. Langmuir, 20: 3528-3531.
21. Cullity, B.D. and S.R. Stock, 2001. Elements of X-ray Diffraction. 3rd Edn., Prentice Hall, New Jersey, ISBN: 0201610914, Pages: 664.
22. Alberti, G., E. Torocca and A. Conte, 1996. Stoicheiometry of ion exchange materials containing zirconium and phosphate. J. Inorg. Nucl. Chem., 28: 607-613.